conference papers

Step bunching in a diffusion-controlled system: phase-shifting interferometry investigation of ferritin

Olga Gliko, Nicholas A. Booth and Peter G. Vekilov

Department of Chemical Engineering, University of Houston, Houston, TX 77204, USA

We present a novel phase-shifting interferometry technique for investigations of the unsteady kinetics and the formation of spatio-temporal patterns during the protein crystallization. We applied this technique to the ferritin crystal growth, which is controlled by the rate of supply of material. We find strong fluctuations of growth rate, step density and step velocity due to passage of step bunches. The fluctuation amplitudes decrease with higher supersaturation and larger crystal size, as well as with increasing distance from the step sources. Since these are parameters affecting the solute supply field, we conclude that fluctuations are rooted in the coupling of the interfacial processes of growth to the bulk transport in the solution. Analysis of the step velocity dependence on local slope indicates a very weak interaction between the steps. Hence, in diffusion-controlled systems with non-interacting or weakly interacting steps the stable growth mode is that *via* equidistant step trains, and randomly arising step bunches decay.

Keywords: ferritin; protein crystallization; interferometry; kinetic fluctuations; step bunching

1. Introduction

Protein crystals are predominantly used for determinations of the atomic structure of the protein molecules (Burley *et al.*, 1999). Unsteady growth conditions and time-dependent impurity incorporation into growing crystals lead to striae and deterioration of the crystal quality (Chernov, 1984). Besides, inhomogenuities arise even under steady external conditions if intrinsic kinetics instabilities, such as step bunching, occur (Bauser, 1994); bunching has been shown to cause growth striations in lysozyme crystals (Vekilov & Rosenberger, 1998a). To investigate the mechanisms leading to step bunching, an *in-situ* technique with high spatial and temporal resolution is required. Michelson interferometry was successfully applied to the study of growth kinetics and surface morphology of inorganic crystals grown from solutions (Chernov *et al.*, 1986; Kuznetsov *et al.*, 1987; van Enckevort, 1984) and protein crystals (Kuznetsov *et al.*, 1995; Monaco & Rosenberger, 1993; Vekilov *et al.*, 1993). While inferior in spatial resolution to atomic force microscopy, this technique is non-intrusive and allows imaging and monitoring of entire crystal faces. The development of phase-shifting interferometry, discussed below, has significantly increased the depth and time resolution (Onuma, 1994).

The kinetics instabilities and step bunching during the crystallization of the protein lysozyme were studied using a high-resolution interferometry technique (Vekilov *et al.*, 1995a). It was concluded that fluctuations are intrinsic and result from the coupled bulk transport and interfacial kinetics processes (Vekilov *et al.*, 1996). According to the mechanism put forth in these works, the strongest instabilities occur when the growth proceeds under equal weights of the transport and kinetics in the overall rate control. Hence, shifts towards purely kinetic, or, conversely, purely diffusive regimes should lead to higher stability. A numerical model of coupled bulk transport and nonlinear interfacial kinetics was developed and evaluated with parameters taken from lysozyme crystallization, dominantly controlled by interfacial kinetics (Lin *et al.*, 1996; Rosenberger *et al.*, 1999; Vekilov *et al.*, 1997); the model quantitatively reproduces the experimentally observed unsteadiness. Changing the system parameters toward stronger kinetics control decreases the fluctuation amplitudes, while stronger step kinetics nonlinearities (step-step interactions, asymmetry for incorporation from the top and lower terraces (Ehrlich & Hudda, 1966; Schwoebel & Shipsey, 1966), stochastic generation of new crystalline layers, etc.) increase them. Further experiments with lysozyme utilizing forced solution flow show that faster convective solute transport, which shifts the working point towards kinetic control, resulting in reduced fluctuations (Vekilov & Rosenberger, 1998b).

If the rationale, developed based on lysozyme data, holds, in crystallization systems with dominant transport control, such as ferritin, a shift of the working point toward slower transport should dampen the fluctuations. Ferritin is a suitable system for studies of non-linear dynamics—the molecular mechanisms of ferritin crystallization and defect formation has been elucidated to a certain detail using atomic force microscopy (Yau *et al.*, 2000a). Thus, the aim of the investigations discussed here is to test if ferritin growth is steady or unsteady, and in the latter case, to experimentally study the origin of kinetics unsteadiness. We search the answer to this question in the dependencies of the amplitude of local slope fluctuations on the parameters affecting transport to the interface: supersaturation, crystal size and location on the crystal faces. For the experiments we developed a novel phase-shifting interferometry setup, which differs from those described in the literature by the different optical and image processing schemes employed.

2. Materials and methods

2.1. Phase-shifting interferometry

A schematic diagram of the phase-shifting Michelson interferometer is presented in Figure 1. The linearly polarized light from a $\lambda_{laser} = 6328$ nm He-Ne laser passes through a spatial filter consisting of a short-focus objective lens, a 10 µm pinhole and a long focus objective lens. In this way, specs are filtered out, the beam is broadened to a ratio equal to the ratio between the two focal lengths, and an area of practically uniform intensity in the center of the broadened beam is achieved (Chernov *et al.*, 1986). Collimation
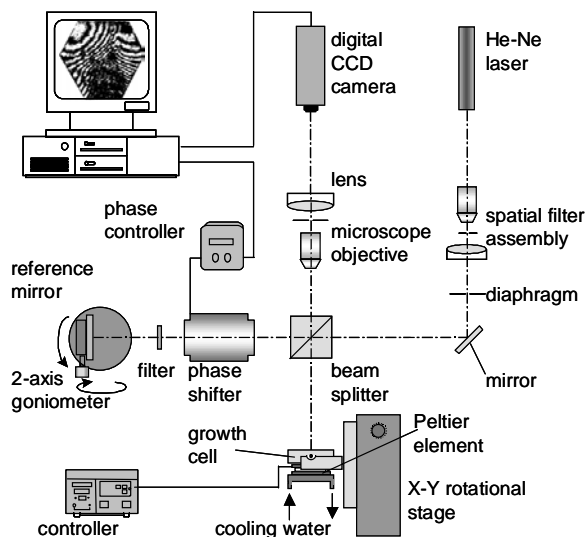

Figure 1
Schematic of the experimental setup of phase-shifting interferometry.

of the output beam is achieved by fine-tuning the position of the long-focus lens along the optical axis. To minimize parasitic reflections from excess laser light in the optical pathway, a variable aperture diaphragm is placed after the spatial filter assembly that limits the beam width to 7 mm.

The beam is then divided into two arms by a beam splitter (Oriel). The surface of growing crystal reflects one of the arms, while a high flatness mirror (Newport) is used in the reference arm. As emphasized below, uniform intensity along the cross section of the two beams is a crucial requirement for quantitative surface characterization. This is achieved by using high quality optical components, and by careful alignment of all optical components using mechanical mounts with micrometer-scale adjustments. Ultimately, the depth resolution of the method is determined by the flatness of the reference mirror. While minimal roughness mirrors that ensure non-uniformities of < 5 Å on a 1 μm scale are easy to acquire, the best serially produced mirrors have a guaranteed flatness of "1/20 of the wavelength". By placing two such mirrors in the interferometer and processing the data as described below, we found this to mean a wavy surface with characteristic amplitudes of about 5–10 nm and a wavelength in the range 10–100 μm.

To introduce the phase shift, we placed a liquid crystal variable retarder (Meadowlark Optics) in the reference arm. This "phase-shifter" operates by discretely changing the applied voltage to an element containing nematic liquid crystals to vary their refractive index. As a result, the optical pathway of the reference beam is varied, and this shifts the phase of the interferograms.

The interference pattern is magnified by a Leica MZ9 microscope. The variable zoom of the microscope allows magnifications in the range 12 × to 120 ×. The lower zooms were used during alignment of the optical subsystem; the highest zoom ratio was employed for data collection. An aperture with a radius of ~ 1mm is placed in the focal plane of the microscope objective to block unwanted reflections from surfaces in the optical pathway. This diaphragm is another crucial component for reliable quantitative data.

The images are acquired by a CCD video camera (Kodak Megaplus) with a 1024 × 1024 resolution, 10 bit B&W acquisition (corresponding to 1024 levels of gray), and frame rate of 4 frames/s.

The microscope and all optical components are mounted on a floating optical table. To minimize thermo-mechanical dimensional changes of the two arms of the interferometer that could be misconstrued for growth, the optical table is placed into a styrofoam enclosure with a clear vinyl shroud as a front access port. The air temperature in the enclosure is stabilized to within 0.1°C, which requires stabilization of the laboratory temperature within 1°C (Vekilov *et al.*, 1995a).

2.2. Solution preparation and growth cell

The crystallizing solution contains between 2–2.5 mg/mL horse spleen ferritin purchased from Sigma and purified to reduce the level of the most common impurity, the covalent dimer of ferritin, to below 5% (Thomas *et al.*, 1998). We use 2.0 % (w/v) = 0.1 M CdSO$_4$ as a precipitant and 0.2 M sodium acetate buffer (NaCH$_3$COO) to fix the pH at 5.05. The supersaturation is calculated as $\sigma = \ln(\gamma C/\gamma_e C_e) \approx \ln(C/C_e)$, where C is the concentration of the solution, $C_e = 35 \mu$g/mL (K. Chen, unpublished) is the solubility.

A 10 μL droplet of crystallizing solution is placed at the center of a Teflon plate, which is then covered and sealed to prevent solvent evaporation. After several crystals nucleate (1-3 days), this plate is transferred to the bottom of growth cell, and additional 35 μL of crystallizing solution are added. The drop is covered by a glass slip, resulting in the formation of a liquid bridge between the cell bottom

and the glass cover. To minimize unwanted interference fringes, the cell body is designed so that the cover glass is tilted from the horizontal plane. The temperature of the solution in the growth cell is stabilized to 23 ± 0.01°C by a thermoelectric (Peltier) cooler. A thermocouple, embedded in the cell holder, measures the temperature and is connected to the controller of the thermoelectric cooler (Marlow Industries). The heat from the thermoelectric cooler is dissipated to cooling water circulating through the cell support. The cell support can be tilted up to 30° about two horizontal axes to align a chosen crystal face normal to the incident beam.

A small mirror is attached atop the cell holder. The intensity recording from this mirror allows us to register dimensional changes within interferometer and uncontaminate the signal due to shifts of the growth of the investigated crystal face (Vekilov *et al.*, 1995a).

Under the chosen conditions, the ferritin crystals are always faceted by octahedral {111} faces. Typically, 2-10 crystals form in a droplet and sediment to the Teflon bottom driven by gravity. They continue to grow and fill the micro-voids in the Teflon substrate; as a result, the crystals are firmly attached to the cell bottom. Such firm attachment is necessary for a successful alignment of the crystal face perpendicular to the object beam of the interferometer.

2.3. Data collection and processing

We employ a five-step phase-shifting algorithm. A sequence of five interferograms is recorded and digitized. In the sequence, the interferograms differ by a π/2 optical phase shift, introduced into the reference beam between each of sequentially recorded interferograms. For this type of data collection, the computer sequentially saves an image to the random-access memory, triggers a change in the voltage to the phase-shifter pre-determined by the calibration routine discussed below, saves another image, and so on.

To ensure that the phase-shifter introduces phase variations of π/2 between the recorded interferograms, a correlation between the applied voltage and the introduced retardation is established. For this calibration, we placed the liquid crystal element of the phase-shifter between a pair of crossed polarizers and determined the intensity transmitted by the phase-shifter as a function of the applied voltage. The minimum and maximum in transmission correspond to phase shifts 0 and 2π, respectively; the voltages required for the other phase shift values were determined by interpolation on the transmitted intensity axis. With a properly calibrated phase-shifter, the unwrapped and the differential phase and surface height profiles, see below, do not exhibit any traces of the interference fringes.

In each of the five interferograms, the interference intensity at a point (x, y) is described by

$$I_i(x, y) = I_r + I_c + 2\sqrt{I_r I_c} \cos[\phi(x, y) + \delta_i] \qquad (1)$$

where I_r and I_c are the intensities of the reference and crystal beams, respectively. We split the phase difference into two components: $\phi(x, y)$ is the phase difference attributed to the deviations of the crystal surface from ideally flat and parallel to reference mirror, while δ_i is the phase difference introduced by the phase-shifter. The phase shift δ_i takes on five discrete values:

$$\delta_i = 0, \pi/2, \pi, 3\pi/2, 2\pi; \qquad i = 1, 2, 3, 4, 5 \qquad (2)$$

Eq 1 can be solved for the phase difference $\phi(x, y)$:

$$\phi(x, y) = \tan^{-1}\left[\frac{2(I_2 - I_4)}{2I_3 - I_5 - I_1} \right] \qquad (3)$$

with each $I_i = I_i(x, y)$. This phase distribution is stored as a grayscale image.

The resulted distribution of phase values has discontinuities of magnitude π due to the nature of arctangent function. The phase calculation routine introduces truncation errors around the discontinuities–neighboring points that are likely to possess similar phases are assigned to different domains. To reduce these errors, we employ a "salt-and-pepper" filter, which compares the phase value at each pixel with the average of the eight neighboring pixels and if the difference is greater than $3\pi/4$, replaces the original value with the average. The final phase distribution is then obtained by unwrapping the phase to remove the π discontinuities.

The calculated phase is related to the crystal surface height $h(x,y)$:

$$\phi(x,y) = \frac{4\pi n h(x,y)}{\lambda} \qquad (4)$$

where n is the refractive index of the protein solution and λ is the laser wavelength. Using this expression we reconstruct the microscopic morphology relief of the growing crystal surface.

For rectangular sections of the surface where the local slope does not change sign, we obtain a differential image by subtracting the average slope. The differential images clearly reveal the local slope variations, i.e., step bunching.

The phase-shifting interferometry technique discussed above was applied to monitor the dynamics of steps during the growth of crystals of the protein ferritin. Figure 2 shows the morphology of (111) faces of two ferritin crystals of sizes 200 μm and 470 μm. Figure 2a–e presents five interference images of the growing crystal surface collected with a phase shift increasing by $\pi/2$ between two neighbors in the sequence. The first and fifth frames appear identical, because of the accumulated 2π shift between them. With the chosen magnification of the optical system, each pixel in an image corresponds to 1×1 μm^2 area of the crystal surface. The time taken to capture five-image sequence is about 1 s. Because the tangential growth rates of ferritin do not exceed the value of 40 nm/s in our experiments, fringes do not move from one pixel to another during this time.

The "phase-wrapped" image calculated using Eq 1 is shown in Figure 2f, g. The gray scale is proportional to the surface height. The discontinuities result from the calculation algorithm based on the tan$^-$^{1} function and correspond to a height difference of $\lambda_{laser}/4n$; $n = 1.3320$ is the refractive index of the solution, largely determined by its acetate and CdSO$_4$ components (Fredericks et al., 1994) and measured as in (Petsev et al., 2000).

A second data collection routine is based on the intensity of the interference image at up to 10 locations recorded over periods of several hours with a time resolution of 1 s. The traces are processed to obtain the values of normal growth rate, local slope and step velocity, as described earlier (Vekilov et al., 1995a).

3. Results and discussion

3.1. Phenomenology of the time-dependent kinetics

During the growth of ferritin crystals the growth layers are always generated by 2D-nucleation; for reviews on this and alternative mechanisms see, e.g., (Malkin et al., 1996; Vekilov & Alexander, 2000). For small crystal sizes and supersaturations $\sigma < 3$, the distribution of 2D-nuclei is uniform across the whole face and the face remains flat on a macroscopic scale as the crystal grows. For higher supersaturations and crystals larger than 100 μm, 2D-nucleation localizes at the facet edges and corners. Numerical modeling of diffusive-convective transport of crystallizing proteins has linked this localization to higher interfacial supersaturation at the edges (Lin et al., 1995; Lin et al., 2001). Furthermore, the model calculations showed that the nonuniformity in interfacial

supersaturation increases with the size of the crystal and the bulk solution supersaturation.

Figures 3a–c show the time traces of the normal growth rate R, the local slope p, and step velocity v recorded at the marked location near the facet center in Figure 2g at $\sigma = 4.3$. R, p, v fluctuate by up to 100% of their respective average values. The fluctuations of local slope, which is proportional to the step density, indicate that the unsteadiness occurs through the formation of patterns of lower and higher step density, step bunches. In order to analyze the fluctuations dependencies on different factors such as supersaturation, crystal size, location on the facet, we use a Fourier decomposition of the three time traces. Earlier work has shown that the Fourier frequencies, characterizing the fluctuation time scales, and the Fourier amplitudes, corresponding to the deviations from average values of the respective kinetic variables, are reproducible characteristics of the unsteady behavior and only depend on the external conditions (Vekilov et al., 1996). We use the Fourier transform in the form

$$R(t) = \sum_m A_m \cos\left(\frac{2\pi n}{T}t + \varphi_m\right), \quad m \geq 0 \qquad (5)$$

where A_m, $2\pi n/T = f_m$ and φ_m are the m-th ($m = 0, 1, \ldots$) Fourier amplitude, frequency and phase, respectively, T is the total length of
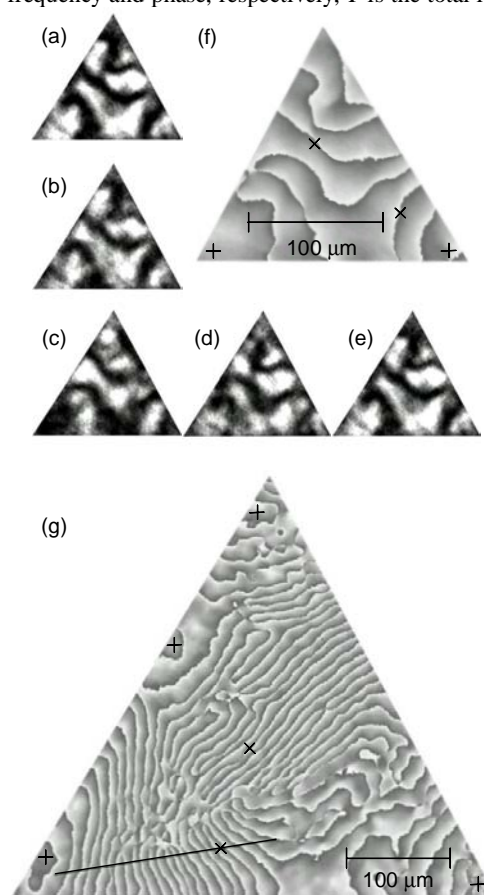

Figure 2
Typical morphology of a (111) face of a ferritin crystal. (a–e) A sequence of five interferometric images from the surface of ferritin crystal recorded with a phase shift of $\pi/2$. (f, g) The phase-wrapped images. The difference in height between the brightest and darkest pixels is $\lambda/4n = 0.119$ μm. (f) $\sigma = 4.0$, (g) $\sigma = 4.3$. +, locations of layer generation; ×, locations of growth kinetics monitoring; solid line indicates locations of surface features quantification, discussed further in the text.

the monitoring period. All A_m's have the dimension of the growth rate R and A_0 equals the averaged growth rate, R_{avg}. The Fourier spectra of the time traces of local slope $p(t)$ and step velocity $v(t)$ are calculated in an equivalent fashion. Figures 3d–f present the normalized Fourier spectra $A(f_m)/A_0$ of $R(t)$, $p(t)$ and $v(t)$. The Fourier frequencies are inversely proportional to the characteristic time scale Δt of the fluctuations.

3.2. Step-step interactions

Figures 3d–f show that the Fourier spectra for R, p, and v are similar. In particular, the R and p spectra reach their maximum amplitudes at the same frequency $f = 0.001$ s^{-1}, which corresponds to a fluctuation with $\Delta t \cong 17$ min. Since the Fourier spectra of p directly reflect the step bunching, we will use only these spectra in the further considerations.

As shown in Figures 3a–c, the fluctuations are rather periodic. However, there appears to be no correlation between the fluctuations of the slope and the step velocity. For further insight, we apply to following considerations. The dependence of the step velocity on the local slope and the reduced concentration $(C - C_e)C_e^{-1}$ can be expressed in a very generic form as (Vekilov *et al.*, 1995b)

$$v = \frac{b_{step}(C - C_e)/C_e}{1 + kp} \qquad (6)$$

where b_{step} is an effective step kinetic coefficient and k is a parameter characterizing the step-step interactions. For non-interacting steps, $k = 0$; for strongly interacting steps such as those in lysozyme growth, where the incorporation into steps is preceded by slow diffusion through the solution bulk and the terraces between the steps, k is in the range 1000–2000 (Vekilov *et al.*, 1995b; Vekilov *et al.*, 1996); for the growth of inorganic phosphates with a similar growth mechanism, values of k are ~1000 (Booth *et al.*, 2002; Vekilov *et al.*, 1992).

Prompted by the form of the $v(p)$ dependence in Eq 6, we plot the reciprocal step velocity $1/v$ as a function of the local slope p for a trace recorded over several hours at the location near the center of facet in Figure 2g. To extract the deterministic link between v and p, we calculate the least square fit of the data to a straight line. From extrapolated intercept of this line with the ordinate axis and the known value of $(C - C_e)/C_e = 71$, we obtain the value of $b_{step} = 4.8 \times$
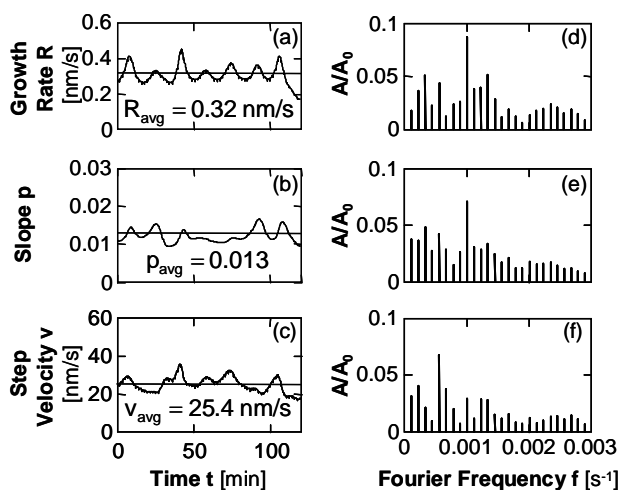
10^{-8} cm/s. The step kinetic coefficient $\beta = b_{step}/\Omega C_e = 11 \times 10^{-4}$ cm/s (Ω is the crystal volume per molecule, $\Omega C_e = 4.2 \times 10^{-5}$) is somewhat higher than the value of $\beta = 6 \times 10^{-4}$ cm/s obtained using AFM (K. Chen, unpublished). From the slope of the fit, we calculate $k = 32$ and $kp_{avg} \approx 0.35$. This low value of k indicates a very weak interaction between steps, i.e. the diffusion supply fields around the steps do not overlap. This makes the ferritin system quite different from lysozyme, which is characterized by strong interaction between steps, which results in dependence of step velocity on slope (Vekilov *et al.*, 1995b).

3.3. Variations of the fluctuation patterns with the external conditions

Figure 4 presents the Fourier spectra of slope traces recorded at two locations on the facet shown in Figure 2g. The maximum values of the Fourier amplitudes are shown on the plots. Comparison of the spectra shows that the fluctuation amplitudes decrease as supersaturation increases and are greater near the facet edges than at the facet center. Note that the lower fluctuations at the facet center and at the higher supersaturations occur despite being accompanied by a higher average vicinal slope. This is a remarkable observation, because the average vicinal slope has been identified as a major *destabilizing* factor for equidistant step trains (Chernov *et al.*, 1993). We conclude that the mechanism leading to decay of the fluctuations is sufficiently strong to overpower the average slope effects.

To understand the higher p values at the facet center than those at the facet periphery, see Figure 2g, we note that this interface shape is a result of the facet morphology response to non-uniform nutrient supply (Chernov, 1974), discussed in detail for the case of protein growth in (Lin *et al.*, 1996; Vekilov *et al.*, 1995b). The non-uniformity in local step density compensates non-uniformity in interfacial supersaturation and step velocity. As a result, the normal growth rate R retains uniformity across the facet and the macroscopic flatness of the facet is preserved.

If we compare the steepest segments of a step train away from the crystal edge to the shallowest close to the edge, for instance along the line in Figure 1g, we would find a ratio of at most two. This ratio equal the ratio of the interfacial concentration of ferritin at the two locations, calculated in ref (Lin *et al.*, 2001), i.e., the slope non-uniformity is completely determined by the surface concentration non-uniformity. This is in sharp contrast to findings with lysozyme, where a 10% surface concentration non-uniformity results in a 4–5× steeper slopes (Lin *et al.*, 1996; Vekilov *et al.*, 1995b). The strong
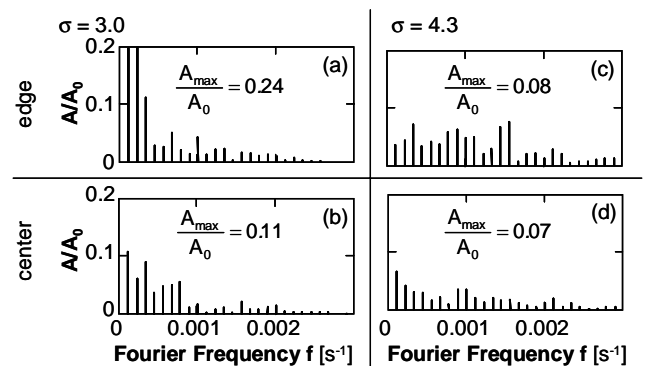
Figure 3
(a)–(c) Time traces of the normal growth rate R, the local slope p and the step velocity v recorded during growth of ferritin crystal at supersaturation $\sigma = 4.3$. (d)–(f) corresponding normalized Fourier spectra, for definitions, see text; in (d)–(f), the zero-th normalized amplitude, $A/A_0 = 1$ at $f = 0$ is omitted.

Figure 4
Fourier spectra of traces of the local slope p for the crystal of a 470 μm size shown in Figure 2g. (a) $\sigma = 3.0$, monitoring location at the facet edge, $p_{avg} = 0.006$; (b) $\sigma = 3.0$, monitoring location near the facet center, $p_{avg} = 0.008$; (c) $\sigma = 4.3$, edge, $p_{avg} = 0.012$; (d) $\sigma = 4.3$, center, $p_{avg} = 0.014$.

enhancement of the surface morphology response was attributed to the strong step-step interaction in lysozyme; the observations with the weakly interacting steps on ferritin lend strong support to this mechanism.

We calculated the Fourier spectra of slope traces recorded at the center of two facets with different size (Figures 2f and 2g) at the same supersaturation $\sigma = 4.0$. The maximum amplitude value is significantly higher for the smaller crystal, while the averaged slope is lower in this case 0.005, compared to 0.013.

We also compared the Fourier spectra of slope traces recorded simultaneously at two different locations of the facet shown in Figure 2f. The first location is close to the location of layer generation near the facet corner, while the second is further removed from the layer source. The amplitude of the slope fluctuations increases with the distance from layer source, while, as above, the averaged value of the slope decreases.

To understand these observations, we use that the crystal size, the location on the facet and the supersaturation are parameters that strongly affect the solute supply to the interface. Hence, the observed dependencies of the fluctuation amplitudes with these parameters indicate that, similar to lysozyme (Vekilov *et al.*, 1996), the growth instability is due to the coupling of the nonlinear interfacial processes of growth to the bulk transport in the solution.

However, in all studies of ferritin, the dependence of the fluctuation amplitudes on the respective parameter is opposite to that for lysozyme, and may appear counterintuitive. Thus, we would expect the faster growth at higher supersaturations to be more instable and with stronger fluctuations, we would expect the instabilities to evolve as the steps propagate down their pathway, and so on. This last controversy provides the key to understanding the unsteady behavior of the step trains in ferritin growth. Indeed, if the fluctuation amplitudes are dampened as the steps move on, it follows that the stable state, towards which the step train is converging, is the equidistant step train. Along this line of thought, we must conclude that the step bunches are generated at the location of step generation, i.e., the 2D nucleation process is highly unsteady, and consist of spurts of nucleated layers, leading to stacks of steps, followed by lower activity. The dependence of the fluctuation amplitudes on the supersaturation in the solution bulk suggests that the unsteady layer generation is caused by its coupling to the solute supply to the location of step generation. This coupling makes the nucleation process intrinsically unstable—an increase in the layer generation leads to solution depletion, a strong drop in the 2D nucleation rate, fewer nucleated steps that allow replenished supersaturation, and so on.

To test this model of nucleation caused by step bunching, we expended the model of coupled bulked transport and interfacial kinetics processes, discussed in (Lin *et al.*, 2001) to include layer generation and step propagation (Lin, unpublished). The simulations results confirmed the suspected highly unsteady generation of layers at the facet edges.

The non-uniform step generation at the facet edges produces the step bunches. As the steps move away from their sources towards the facet center, the step bunches decay. An important factor for this decay is the lack of step-step interactions—such interactions are known to strongly destabilize the uniform step trains, and lead to increasing fluctuations (Vekilov *et al.*, 1997).

Another potential destabilizing factor could be impurity action. The main impurities in this system are the covalently bound ferritin dimers (Thomas *et al.*, 1998). Previous work by AFM has found that despite their relatively high surface concentration, $\sim 2.2 \times 10^9$ cm^{-2} (Yau *et al.*, 2001), the dimers do not affect the motion of steps (Yau *et al.*, 2000b). The reason for this is that the mean distance between two dimer molecules adsorbed on the surface, $\sim$200–300 nm, is higher than the critical 2D radius, of the order of several molecular

diameters, i.e., 50–100 nm. As a consequence, the dimers do not affect step motion, and do not enhance step bunch formation.

Since neither of these potential destabilizing mechanisms is acting, the motion of steps and the evolution of the step bunches formed at the stage of layer generation is only affected by the coupled bulk transport and surface kinetics. To identify which of the two coupled processes dominate the rate control, we evaluate the kinetic Peclet number, introduced in (Vekilov *et al.*, 1996) as the ratio

$$Pe_k = \beta p \delta / D \qquad (7)$$

where D is the diffusivity of the ferritin $= 3.2 \times 10^{-7}$ cm^2/s (Petsev *et al.*, 2000), and δ is the characteristic diffusion layer thickness, typically of the order of 200 μm. Using the values of b and p discussed above, we get $Pe_k \approx 1.0$, i.e., ferritin growth is predominantly controlled by the transport in the solution. For such systems, the rationale predicts higher stability at *even higher* relative weight of transport. Thus, we should expect lower kinetic fluctuations at higher supersaturations, at larger crystals sizes, and at the facet centers. This is in exact correspondence with the experimental findings discussed above. We conclude that the observations with ferritin support the mechanism of generation of the step bunches and the associated rationale for the control of the kinetics instabilities in layer growth systems.

3.4. Spatial-temporal characteristics of the step patterns

The phase-shifting technique allows reconstruction of the surface morphology. Figure 5a shows the height profile along the line depicted in Figure 2g. The height decreases as the distance from layer sources increases. The corresponding slope profile and its spatial Fourier spectrum are shown in Figure 5b and c, respectively. The wave numbers in Figure 5c are reciprocal to the corresponding step bunch wavelengths λ. The maximum amplitude occurs at a wave number of 0.045 μm^{-1} corresponding to fluctuations with λ_{max}
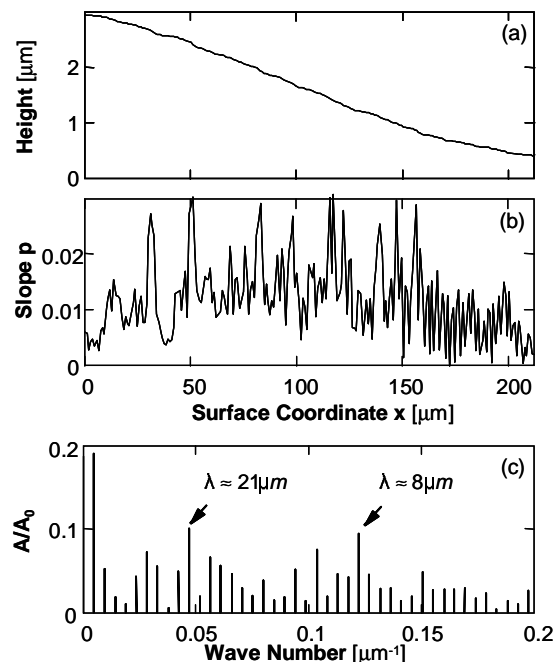

Figure 5

(a) Height and (b) local slope profiles along the line shown in Figure 2g. (c) Corresponding Fourier spectrum of *p*. The characteristic step bunch wavelengths λ are indicated in the plot. The first amplitude in (c) corresponds to the overall bending of the surface seen in (b).

~21 μm. From the time traces measured at the location on the profile line at the same σ = 4.3, see Figure 4c, we determine the characteristic step bunch frequency f_{max} = 0.0016 s^{-1} (Δt ~ 10.7 min).

From these two values, we can evaluate the step bunch velocity as $v_{bunch} \approx \lambda_{max} f_{max}$ ~ 33 nm/s. The value of v_{bunch} is close to the mean step velocity under those conditions, $v \approx$ 35 nm/s. Thus, in the case of non-interacting steps, the step bunches move with the same velocity as elementary steps.

4. Conclusions

We have shown that under steady growth conditions, ferritin growth kinetics is highly unsteady and the fluctuation amplitudes reach up to 100% of the average values of the growth rate, the step density and the step velocity. The variations in the local slope indicate that the fluctuations reflect the dynamics of formation and evolution of step patterns. The lack of correlation of the step velocity and local slope indicates very weak step-step interactions. Correspondingly, the propagation rate of step bunches is same as the elementary step velocity.

From the dependencies of the amplitude of local slope fluctuations on the supersaturation, crystal size and location on the facet we conclude that the unsteady growth is the result of the coupling between solute transport towards the interface and the nonlinear interfacial kinetics. The main factor introducing non-linearity onto the interfacial kinetics is the generation of layers via a 2D nucleation mechanism, with its suspected exponential dependence on the supersaturation. We find that the fluctuation amplitude decreases with increasing distance from the layer sources. Hence, for non-interacting steps growing under diffusion control the step bunches decay and the step train tends towards its stable, equidistant state.

These findings in a transport-controlled system provide a strong support to the rationale for the control of the step bunching instabilities in layer growth systems that was previously based only on observations with a kinetically controlled system.

References

Bauser, E. (1994). Atomic Mechanisms in Semiconductor Liquid Phase Epitaxy. In *Handbook of Crystal Growth* (Hurle, D. T. J., ed.), Vol. 3b, pp. 879-911. North Holland, Amsterdam.

Booth, N. A., Chernov, A. A. & Vekilov, P. G. (2002). *J. Cryst. Growth.* In the press.

Burley, S. K., Almo, S. C., Bonanno, J. B., Capel, M., Chance, M. R., Gaasterland, T., Lin, D., Sali, A., Studier, F. W. & Swaminathan, S. (1999). *Nature Genet.* **23**, 151-157.

Chernov, A. A. (1974). *J. Cryst. Growth*, **24/25**, 11-31.

Chernov, A. A. (1984). *Modern Crystallography III, Crystal Growth,*, Springer, Berlin.

Chernov, A. A., L, N., Rashkovich & Mkrtchan, A. A. (1986). *J. Cryst. Growth*, **74**, 101-112.

Chernov, A. A., Coriell, S. R. & Murray, B. T. (1993). *J. Cryst. Growth* **132**, 405-412.

Ehrlich, G. & Hudda, F. G. (1966). *J. Chem. Phys.* **44**, 1039-1052.

Fredericks, W. J., Hammonds, M. C., Howard, S. B. & Rosenberger, F. (1994). *J. Crysl Growth*, **141**, 183-192.

Kuznetsov, Y. G., Chernov, A. A., Vekilov, P. G. & Smol'skii, I. L. (1987). *Sov. Phys. Crystallogr.* **32**, 584-587.

Kuznetsov, Y. G., Malkin, A. J., Geenwood, A. & McPherson, A. (1995). *J. Struct. Biol.* **114**, 184-196.

Lin, H., Rosenberger, F., Alexander, J. I. D. & Nadarajah, A. (1995). *J. Cryst. Growth*, **151**, 153-162.

Lin, H., Vekilov, P. G. & Rosenberger, F. (1996). *J. Cryst. Growth*, **158**, 552-559.

Lin, H., Petsev, D. N., Yau, S.-T., Thomas, B. R. & Vekilov, P. G. (2001). *Crystal Growth Des.* **1**, 73-79.

Malkin, A. J., Kuznetsov, Y. G., Land, T. A., DeYoreo, J. J. & McPherson, A. (1996). *Nature Struct. Biol.* **2**, 956-959.

Monaco, L. A. & Rosenberger, F. (1993). *J. Cryst. Growth*, **129**, 465-484.

Onuma, K., Kameyama, T., Tsukamoto, K. (1994). *J. Cryst. Growth*, **137**, 610-622.

Petsev, D. N., Thomas, B. R., Yau, S.-T. & Vekilov, P. G. (2000). *Biophys. J.* **78**, 2060-2069.

Rosenberger, F., Lin, H. & Vekilov, P. G. (1999). *Phys. Rev. E*, **59**, 3155-3164.

Schwoebel, R. L. & Shipsey, E. J. (1966). *J. Appl. Phys.* **37**, 3682-3686.

Thomas, B. R., Vekilov, P. G. & Rosenberger, F. (1998). *Acta Cryst.* D**54**, 226-236.

van Enckevort, W. J. P. (1984). *Prog. Cryst. Growth Character.* **9**, 1.

Vekilov, P. G., Kuznetsov, Y. G. & Chernov, A. A. (1992). *J. Cryst. Growth*, **121**, 643-655.

Vekilov, P. G., Ataka, M. & Katsura, T. (1993). *J. Cryst. Growth*, **130**, 317-320.

Vekilov, P. G., Monaco, L. A. & Rosenberger, F. (1995a). *J. Cryst. Growth*, **146**, 289-296.

Vekilov, P. G., Monaco, L. A. & Rosenberger, F. (1995b). *J. Cryst. Growth*, **156**, 267-278.

Vekilov, P. G., Alexander, J. I. D. & Rosenberger, F. (1996). *Phys. Rev. E*, **54**, 6650-6660.

Vekilov, P. G., Lin, H. & Rosenberger, F. (1997). *Phys. Rev. E*, **55**, 3202-3214.

Vekilov, P. G. & Rosenberger, F. (1998a). *Phys. Rev. E*, **57**, 6979-6981.

Vekilov, P. G. & Rosenberger, F. (1998b). *J. Cryst. Growth*, **186**, 251-261.

Vekilov, P. G. & Alexander, J. I. D. (2000). *Chem. Rev.* **100**, 2061-2089.

Yau, S.-T., Petsev, D. N., Thomas, B. R. & Vekilov, P. G. (2000a). *J. Mol. Biol.* **303**, 667-678.

Yau, S.-T., Thomas, B. R. & Vekilov, P. G. (2000b). *Phys. Rev. Lett.* **85**, 353-356.

Yau, S.-T., Thomas, B. R., Galkin, O., Gliko, O. & Vekilov, P. G. (2001). *Proteins: Struct. Func. Genet.* **43**, 343-352.